Genetic Algorithm-Based Parameter Identification of a Hysteretic Brushless Exciter Model

Dionysios C. Aliprantis, *Member, IEEE*, Scott D. Sudhoff, *Senior Member, IEEE*, and Brian T. Kuhn, *Member, IEEE*

***Abstract*—In this paper, a parameter identification procedure for a recently proposed hysteretic brushless exciter model is discussed. The model features average-value representation of all rectification modes, and incorporation of magnetic hysteresis in the d-axis main flux path using Preisach's theory. Herein, a method for obtaining the model's parameters from the waveforms of exciter field current and main alternator terminal voltage is set forth. In particular, a genetic algorithm is employed to solve the optimization problem of minimizing the model's prediction error during a change in reference voltage level.**

***Index Terms*—Brushless rotating machines, genetic algorithms (GAs), magnetic hysteresis, measurement, parameter estimation, synchronous generator excitation.**

I. Introduction

BRUSHLESS excitation of synchronous generators offers increased reliability and reduced maintenance requirements [1], [2]. These systems consist of an exciter machine and a rotating rectifier mounted on the same shaft as the main alternator (Fig. 1). This paper presents the parameter estimation procedure for a recently proposed brushless exciter model [3]. This model is more detailed than the widely used IEEE exciter model [4]. It features an average-value representation of the exciter–rectifier configuration that is valid in all rectification modes [5], [6], and the incorporation of magnetic hysteresis using Preisach's theory [7], [8].

The exciter is a synchronous machine whose "standard" qd-axes model may be characterized independently by a variety of methods [9]. When no slip rings are installed to enable measurement of the rotating armature's quantities, the characterization must be performed at standstill. However, standstill measurements do not always correspond to actual operating characteristics. For example, the main flux magnetic path may behave differently while rotating. Furthermore, exciter machines are often designed with as little as one slot per pole per phase (as is the case for the machine under test herein), which results in nonsinusoidal winding inductances that require detailed modeling and complicated parameter identification procedures [10].

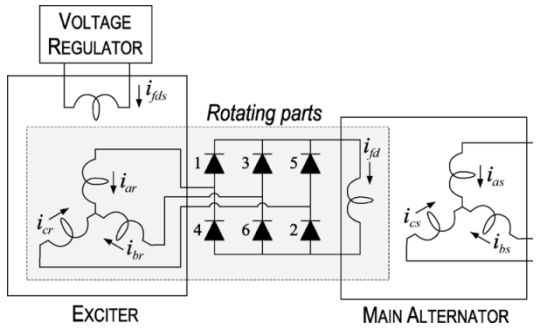

Fig. 1. Schematic of a brushless synchronous generator.

Alternately, if the performance of the exciter-generator system is examined as a whole, a simpler average-value model (AVM) (such as the one proposed in [3]) may be adopted. The model may then be characterized by utilizing the generator's input–output characteristics while rotating. Assuming that the main alternator's model and parameter set are known, this work sets forth a method to extract the exciter's parameters from the measurable quantities, namely, the main alternator voltage and the exciter field winding current.

In general, every parameter estimation procedure aims at finding an optimal parameter vector in the sense that the model's prediction error becomes as small as possible [11]. Identification techniques that are applicable to the IEEE exciter model or, in general, to other linear/linearized time-invariant models [12], [13] are not applicable to the exciter model [3] because this model includes a memory operator—the Preisach hysteresis model. Therefore, its response depends on the time history, and it must be characterized by minimizing a time-domain-based error, as in [14]–[16]. In this paper, a genetic algorithm (GA) is employed for solving this optimization problem.

GAs are loosely based on principles of natural selection and survival of the fittest [17]–[19]. They have proven to be efficient for searching through high-dimensional spaces, and may thus be used as optimization tools, when other optimization algorithms are not sufficient. Some of the major differences between GAs and "conventional" optimization algorithms (e.g., the steepest descent algorithm) are the following.

- The objective function's gradient or Hessian is not required; GAs only use function values.
- The search is guided probabilistically.
- The optimization algorithm operates on a population of solutions (rather than a single solution).

Manuscript received October 28, 2003; revised September 29, 2004. This work was supported in part by the "Naval Combat Survivability" effort under Grant N00024-02-NR-60427 and in part by the Office of Naval Research under Grant N00014-02-1-0990 "Polytopic Model Based Stability Analysis and Genetic Design of Electric Warship Power Systems." Paper no. TEC-00313-2003.

D. C. Aliprantis is with the Greek Armed Forces (e-mail: aliprantis@alumni.purdue.edu).

S. D. Sudhoff is with the Department of Electrical and Computer Engineering, Purdue University, West Lafayette, IN 47907-1285 USA (e-mail: sudhoff@ecn.purdue.edu).

B. T. Kuhn is with SmartSpark Energy Systems, Inc., Champaign, IL 61820 USA (e-mail: b.kuhn@smartsparkenergy.com).

Digital Object Identifier 10.1109/TEC.2005.847967

0885-8969/$20.00 © 2005 IEEE

- An initial guess "close" to the solution is not necessary; population diversity increases the probability of locating the global optimum.
- GAs are amenable to parallel computation; function evaluations may be distributed among separate computers.

For these reasons, GAs are highly suitable for electric machine parameter identification [20]–[24].

II. Notation

Throughout this work, primed stator quantities denote referral to the rotor through the turns ratio, which is defined as the ratio of armature-to-field turns $TR = N_r/N_{fds}$. The transformation of rotating abc to stationary $qd0$ variables is defined by [25]

$$\mathbf{f}^s_{qd0r} = \mathbf{K}^s_r(\theta_r)\mathbf{f}_{abcr} \tag{1}$$

where

$$\mathbf{K}^s_r(\theta_r) = \frac{2}{3}\begin{bmatrix} \cos\theta_r & \cos\left(\theta_r + \frac{2\pi}{3}\right) & \cos\left(\theta_r - \frac{2\pi}{3}\right) \\ -\sin\theta_r & -\sin\left(\theta_r + \frac{2\pi}{3}\right) & -\sin\left(\theta_r - \frac{2\pi}{3}\right) \\ \frac{1}{2} & \frac{1}{2} & \frac{1}{2} \end{bmatrix}. \tag{2}$$

Since a neutral connection is not present, $f_{0r} = 0$.

III. Identification Procedure

The proposed identification procedure is suitable for the brushless exciter model presented in [3]. This model features average-value modeling of all three rectification modes [5], and incorporation of main flux path magnetic hysteresis using Preisach's theory [8]. In particular, transients in the rotor (the armature) are ignored by using a reduced-order machine model formulation. An averaging engine links the qd-axes machine model to the main alternator's field winding. Additional details may be found in the Appendix.

The parameters that need to be identified are

- the exciter's field winding resistance r_{fds};
- the exciter's field winding leakage inductance L_{lfds};
- the exciter's armature winding resistance r_r;
- the exciter's d-axis armature winding leakage inductance L_{ldr};
- the exciter's armature-to-field turns ratio TR;
- the parameters that characterize the exciter's d-axis magnetizing branch; these are related to the Preisach model representation; the selected Preisach function is parameterized by four parameters, namely λ_{Ms}, σ_w, σ_m, $\overline{w}$; also required is the slope of the magnetizing curve at saturation $L_{m,\mathrm{sat}}$;
- the exciter's voltage-behind-reactance q-axis inductance $L_q^{\mathrm{vbr}} = L_{lqr} + L_{mq}$;
- the $v - i$ characteristic of the rotating rectifier diodes.

The resistances, diode characteristic, and turns ratio may be measured at standstill, by disconnecting the exciter and rectifier from the main generator. The remaining eight parameters will be identified from the system's time-domain response.

This section describes the experimental identification procedure as applied to the exciter machine of a 59-kW, 600-V, Leroy–Somer brushless synchronous generator, model LSA-432L7 (Fig. 8). The exciter is an eight-pole machine, whose field is rated for 12 V, 2.5 A. The generator's prime mover is a 110-kW, vector-controlled, Dyne Systems induction motor-based dynamometer, programmed to maintain constant rated speed (1800 r/min). The voltage regulator uses a proportional-integral control strategy to maintain the commanded voltage [560 V line-to-line, fundamental root mean square (rms)] at the generator terminals; the brushless exciter's field current is controlled with a hysteresis modulator. Additional information about these devices and their models may be found in [24], [26] and [27]. (In particular, the voltage regulator model and control diagram is described in detail in Appendix D of [27].)

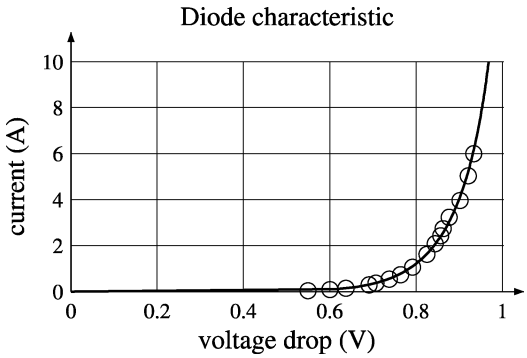

Fig. 2. Static $i - v$ rotating rectifier diode characteristic: measured points and fitted curve.

A. Resistance Measurements

The first step in the characterization procedure is the measurement of the dc values of armature and field winding resistance. Using a four-wire measurement technique, these were determined to be $r_r = 0.121\ \Omega$ and $r_{fds} = 4.69\ \Omega$ at room temperature. The variation of resistance with temperature is not incorporated in the model.

B. Diodes Characterization

The diodes' static voltage-current characteristic is represented by the following function:

$$v_d(i_d) = ai_d + (bi_d)^c. \tag{3}$$

The parameters a, b, and c are obtained with a curve-fitting procedure to experimental points: $a = -4.61 \cdot 10^{-3}$, $b = 0.114$, and $c = 0.109$. The data points and fitted curve are displayed in Fig. 2.

The incorporation of the diodes' voltage drop in the model is significant. For example, consider Mode IV [3], wherein a short-circuit appears across the main alternator's field winding. In this case, the field current i_{fd} (which flows through the field resistance, inductance, and two diodes in series) decays with a time constant that is directly related to the diodes' ohmic resistance. Accurate modeling of the diodes implies accurate prediction of the rate of change of i_{fd}, and consequently of the terminal voltage (see, for example, Fig. 5).

C. Turns-Ratio Measurement

The turns ratio is determined with the technique outlined in [24]. This method consists of alternately exciting the exciter's

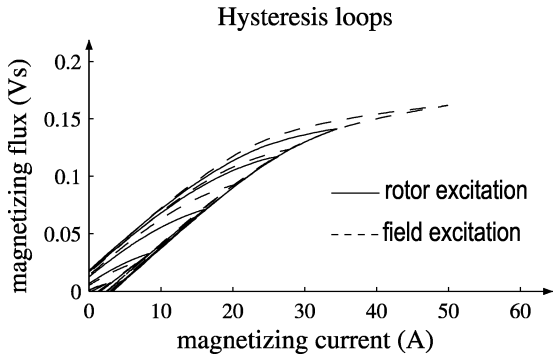

Fig. 3. Hysteresis loop match for $TR = 0.070$.

field and armature windings (input side) with an ac source, while the other side (output side) is open-circuited. The output voltage and the input current are recorded with a dynamic signal analyzer and are processed to obtain hysteresis loops. The tests must be performed at a low frequency in order to ensure that the eddy currents in the rotor circuits are negligible. Herein, the hysteresis loops were obtained at 5 Hz.

The rotor is rotated so that current flowing in the series combination of phases $c - b$ (with phase a open) produces a magnetomotive force (mmf) aligned with the d-axis. When exciting the armature side, terminal quantities are related to qd-axes variables by

$$i_{md} \approx i^s_{dr} = \frac{2}{\sqrt{3}} i_c \tag{4}$$

$$\lambda_{md} \approx \lambda'_{fds} = TR \cdot \lambda_{fds} = TR \int v_{fds} dt. \tag{5}$$

When exciting the field side

$$i_{md} \approx i'_{fds} = \frac{2}{3} \frac{1}{TR} i_{fds} \tag{6}$$

$$\lambda_{md} = \frac{1}{\sqrt{3}} \lambda_{cb} = \frac{1}{\sqrt{3}} \int v_{cb} dt. \tag{7}$$

The integration of the voltage in (5) and (7) is performed numerically. Appropriate integration constants are found such that the loops become symmetric around the origin.

The fundamental idea behind the procedure is to exploit the magnetic nonlinearity properties of the machine's iron. Specifically, different d-axis loops $\lambda_{md}(TR)$ versus i_{md} and λ_{md} versus $i_{md}(TR)$ may be measured by exciting the machine from the armature and the field side, respectively. Each experiment contains a variable that is directly measurable and one that depends on the turns ratio. The turns ratio is a free parameter that is adjusted until a value is found for which the distance between the curves is minimized. This value is quite accurately determined by trial and error. For this machine, $TR = 0.070$ (Fig. 3).

D. Evolutionary Time-Domain Parameter Estimation

In the proposed procedure, the generator is disconnected from the power system and is rotated at 1800 r/min under no-load conditions. The voltage reference is modified according to the profile shown in Fig. 5. These perturbations force the exciter to operate in all three rectification modes and create large variations in its magnetization state, so that the experiment contains enough information for characterizing the model. The quantities of the internal rotating parts (Fig. 1) are not measurable because slip rings were not installed. Therefore, the model is characterized based on terminal quantities only, namely the synchronous generator voltage and the exciter's field current command i^*_{fds}. (In the test system, the actual current closely follows the commanded current.) The GA searches for the parameter set that minimizes the difference between measured and predicted time-domain data. Each individual of the population (i.e., each parameter set) is evaluated by a computer simulation. The model is coded and simulated in Advanced Continuous Simulation Language (ACSL) [28].

In order to quantify the difference between the measured and predicted waveforms, appropriate error functions must be defined. Since it is virtually impossible to achieve perfect synchronization between experimental and simulated ac voltages, the error is based on their envelopes. Specifically, the "envelope" of the line-to-line voltage is defined—based on the synchronous reference frame voltages [25]—as[1]

$$v_{\text{ll,env}} = \sqrt{3\left[\left(v^e_{qs}\right)^2 + \left(v^e_{ds}\right)^2\right]}. \tag{8}$$

The difference at time sample t_k, $k = 1, \ldots, N$ between simulated and experimental waveforms is

$$\Delta v(t_k) = \min\left\{\left|v^{\text{sim}}_{\text{ll,env}}(t_k) - v^{\text{exp}}_{\text{ll,env}}(t_k)\right|, b_v\right\} \tag{9}$$

$$\Delta i(t_k) = \min\left\{\left|i^{*,\text{sim}}_{fds}(t_k) - i^{*,\text{exp}}_{fds}(t_k)\right|, b_i\right\} \tag{10}$$

for the voltage and current, respectively. The constants $b_v = 100$ V and $b_i = 0.5$ A are upper bounds. The error takes into account the maximum and average difference:[2]

$$E_v = \frac{1}{2}\left\{\max\left[\Delta v(t_k)\right] + \text{mean}\left[\Delta v(t_k)\right]\right\} \tag{11}$$

$$E_i = \frac{1}{2}\left\{\max\left[\Delta i(t_k)\right] + \text{mean}\left[\Delta i(t_k)\right]\right\}. \tag{12}$$

The fitness is obtained by a weighted sum of the two errors

$$f = \frac{b_v + w_i b_i}{E_v + w_i E_i} \geq 1 \tag{13}$$

where the weight $w_i = 100$, is used to compensate for the small magnitude of the field current compared to the terminal voltage. The experimental waveforms were sampled every $\Delta t = 1$ ms; the simulated traces were saved at the same rate.

In this work, a GA with real-number encoding of the variables was used. The range of each variable is defined by a minimum and maximum value, and the genes are normalized to the range [0–1]. There are two types of genes: linear and exponential. The exponential gene type is used for searching through spaces that span several orders of magnitude; the GA operates on the logarithm of such variables. The study-specific GA settings are listed

[1]For a three-phase balanced voltage set, $[(v^e_{qs})^2 + (v^e_{ds})^2]^{(1/2)}$ attains a constant value, equal to the peak of the line-to-neutral voltage. Therefore, in this case, $v_{\text{ll,env}}$ is also a constant that corresponds to the peak of the line-to-line voltages. However, in practice, the terminal voltages are not purely sinusoidal; thus creating ripple in the qd-axes synchronous voltages which, in turn, reflects on the waveform of $v_{\text{ll,env}}$

[2]If x_k, $k = 1, \ldots, N$ are the data points of x, then $\text{mean}(x) = (1/N)\sum_{k=1}^{N} x_k$.

TABLE I
LIST OF GA VARIABLES AND SETTINGS

variable	units	gene type	min.	max.	result
λ_{Ms}	Vs	exp.	0.1	2	0.952
$L_{m,\mathrm{sat}}$	mH	exp.	0.5	5	3.37
$\overline{w}$	A	lin.	-50	0	-16.7
σ_w	A	exp.	4	40	10.1
σ_m	A	exp.	4	40	15.9
L_q^{vbr}	mH	exp.	1	5	2.31
L_{ldr}	mH	exp.	0.1	1	0.490
L'_{lfds}	mH	exp.	0.1	1	0.861

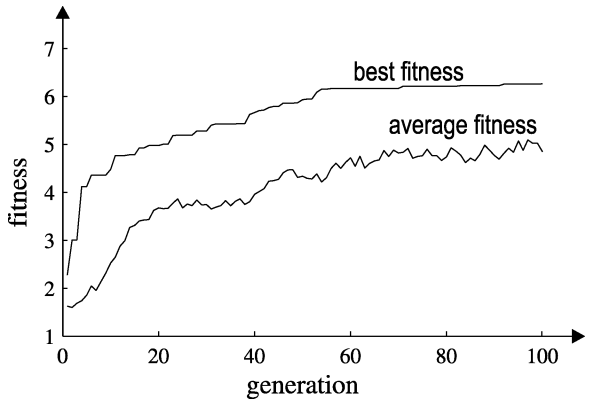

Fig. 4. Plot of fitness versus generation number.

in Table I. The population size was $N_{\mathrm{ind}} = 100$, and evolution was terminated after $N_{\mathrm{gen}} = 100$ generations. The GA has the following structure:

1) initialization (at random) and evaluation of the population;
2) roulette-wheel selection of individuals in the mating pool (preconditioned with sigma-truncation [18]);
3) simulated binary crossover [29] on a gene-by-gene basis with parameter $\eta = 2$ and mating probability $p_{\mathrm{mt}} = 0.6$ per individual;
4) total mutation (where a gene is changed arbitrarily) with probability $p_{\mathrm{tm}} = 0.006\,25 (= 1/8/20)$ per gene;
5) Partial mutation (where a gene's original value is slightly perturbed according to a normal distribution of standard deviation $\sigma_{\mathrm{pm}} = 0.3$) with probability $p_{\mathrm{pm}} = 0.025 (= 1/8/5)$ per gene;
6) evaluation of the individuals' fitness;
7) fitness comparison of the current and previous best individuals. If a fitter individual was not generated, the previous best individual is reinserted in the population (elitism property);
8) random search (a localized search operator that partially mutates the best individual $N_{\mathrm{rs}} = 25$ times according to a normal distribution of standard deviation $\sigma_{\mathrm{rs}} = 0.1$);
9) if the current generation is N_{gen}, then stop; else, go to step 2.

To accelerate the evolution process, the simulations were performed in a parallel computing environment. The evaluations were distributed among a cluster of eight computers (having AMD processors running at 1.67 GHz), and, for 100 generations, approximately 12 h were required.

The evolution of a representative GA run is displayed in Fig. 4. At the specified number of generations, the GA has reached a "plateau," where the fitness increases only incrementally. The achieved fitness [as defined by (13)] was $f = 6.26$. The parameter values of the best individual are contained in Table I. It is possible that if the GA had run for a larger number of generations, then a fitter individual might have been obtained. However, since the predictions of the model with the obtained parameter set were satisfactory, the GA was terminated.

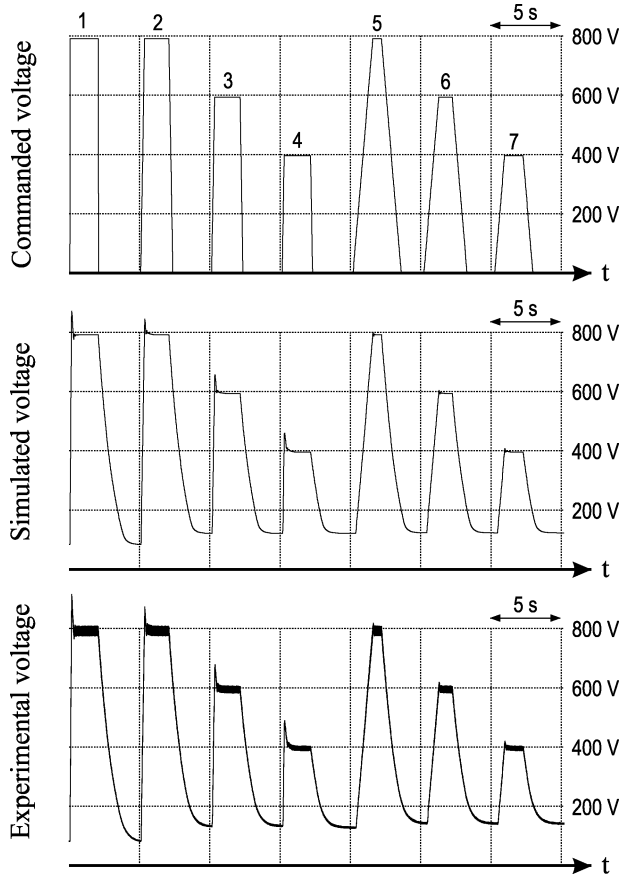

Fig. 5. Plots of the commanded and actual line-to-line voltage "envelope"—no load. Each of the seven trapezoid shaped blocks is characterized by a different slope (the same for rise and fall) and peak voltage: (1) 20 000 V/s, 560 V; (2)–(4) 2000 V/s, 560 V, 420 V, 280 V, respectively; (5)–(7) 400 V/s, 560 V, 420 V, 280 V, respectively.

[Note: the above voltage values correspond to rms quantities.]

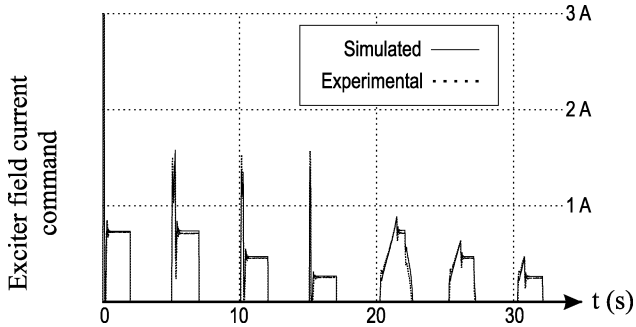

Fig. 6. Plot of the simulated and experimental exciter field current command i^*_{fds}—no load.

The experimental and simulated waveforms of terminal voltage and exciter field current command are illustrated in Figs. 5 and 6, respectively. The terminal voltage exhibits an overshoot, which is more pronounced for the faster slew rate

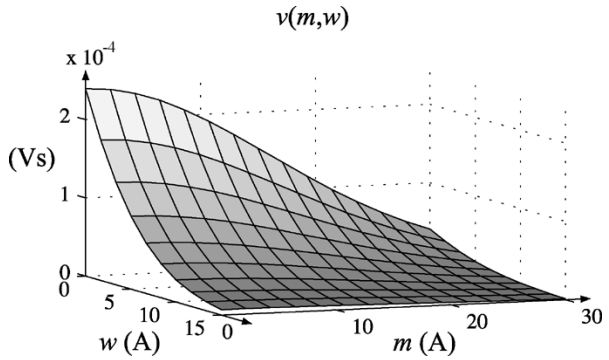

Fig. 7. Preisach function plot for $w > 0$ and $m > 0$. (The function is symmetric with respect to the w-axis.).

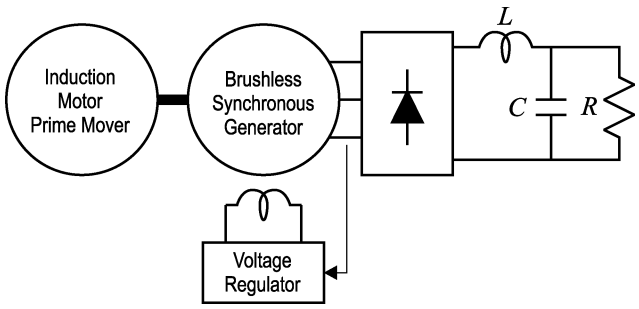

Fig. 8. Schematic of experimental setup; the brushless synchronous generator is feeding a nonlinear rectifier load.

steps. Moreover, due to the exciter's magnetically hysteretic behavior, it does not fall to zero. The varying levels of remanence in the exciter machine reflect on the magnitude of the voltage and are captured with sufficient accuracy. In contrast to the purely sinusoidal simulated voltage, the experimental voltage contains ripple which reflects on its "envelope." This is attributed to main alternator slot effects, not modeled herein [26]. A plot of the obtained Preisach function is shown in Fig. 7.

IV. Model Validation

To validate the model, the generator is connected to a nonlinear rectifier load, as shown in Fig. 8. The load parameters are $L = 7.5$ mH, $C = 500$ μF, and $R = 16.3$ Ω. The same commanded voltage profile (Fig. 5) is applied.

The terminal voltage and exciter field current command are plotted in Figs. 9 and 10, respectively. In Fig. 9, it can be seen that the simulated terminal voltage closely matches the measured voltage for this loaded case, even though the parameter identification was conducted using no-load data. Similarly, in Fig. 10, it can be seen that the simulated and measured field current commands are in good agreement.

V. Conclusion

The brushless exciter model of [3] was successfully parameterized using GAs. The GA minimized an error based on the time-domain difference between the observed and simulated waveforms of the synchronous generator system. The proposed experiment was relatively easy to carry out; it did not require the installation of slip rings for monitoring internal rotating

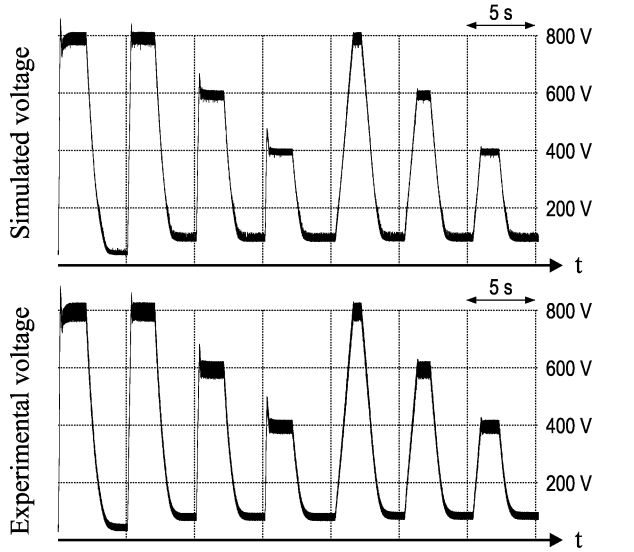

Fig. 9. Plots of the commanded and actual line-to-line voltage "envelope"—loaded case.

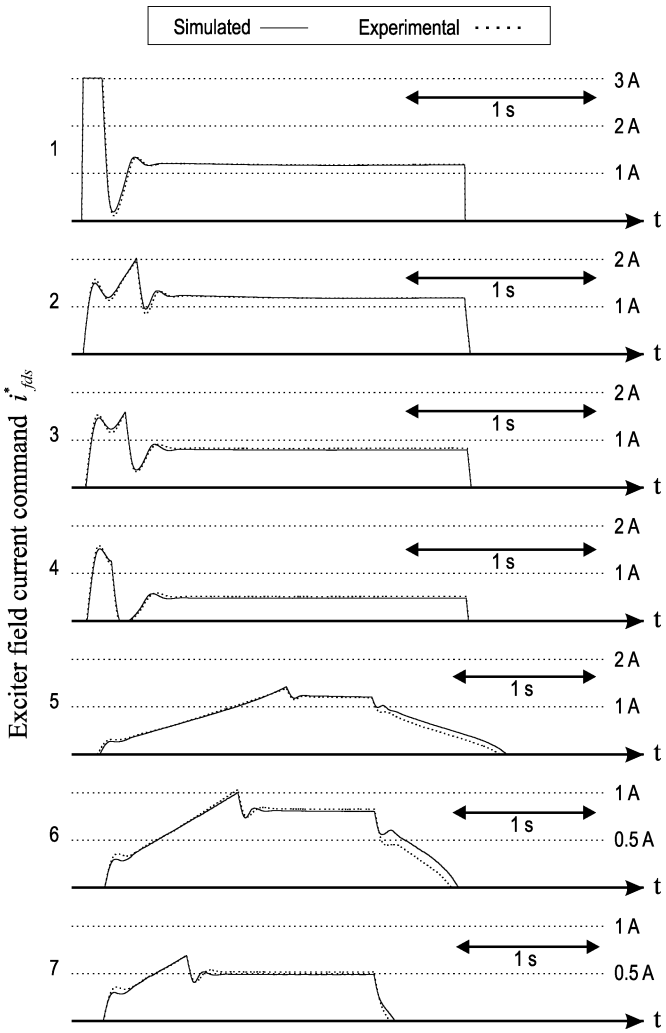

Fig. 10. Plots of the commanded exciter field current i^*_{fds}—loaded case. These correspond to the seven command steps of Fig. 5.

[Note: the first plot depicts a situation where the controller's current limit (3 A) is reached.]

quantities and was performed at no load. The possibility to extract the exciter parameters (as well as the voltage regulator

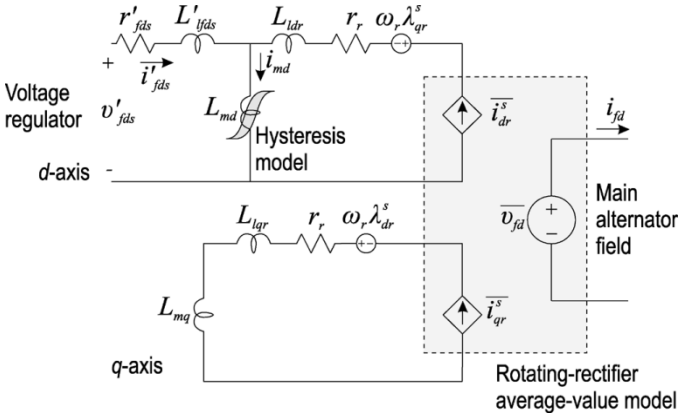

Fig. 11. Exciter's equivalent circuit and interface mechanism to the voltage regulator and main alternator models.

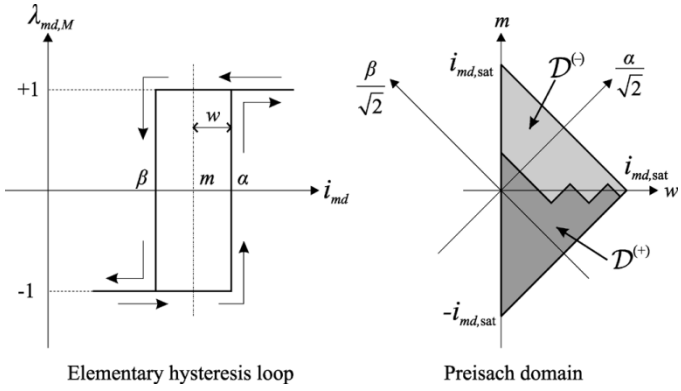

Fig. 12. Illustrations of the elementary magnetic dipole characteristic and the Preisach domain.

parameters) from online data presents an opportunity for future research.

The tremendous potential of GAs (and other evolutionary optimization methods) for parameter estimation has not yet been fully exploited. GAs offer great flexibility to the analyst. In general, a variety of available information about a system (be it in the frequency domain, the time domain, or a combination of both) may be readily incorporated in a fitness function. Furthermore, GAs not only provide means for characterizing complex models, such as the one used herein, but they should encourage the derivation and utilization of more detailed and state-of-the-art models that would otherwise have been intractable to parameterize.

APPENDIX
BRUSHLESS EXCITER MODEL SUMMARY

In the model of [3], the d-axis magnetizing branch contains a hysteretic inductance (Fig. 11), modeled using Preisach's theory [8]. Hysteresis is important because it affects the relationship between exciter field current and generator terminal voltage. The d-axis magnetizing flux is expressed as the sum of two components

$$\lambda_{md} = L_{m,\mathrm{sat}} i_{md} + \lambda_{md,M} \tag{14}$$

where $\lambda_{md,M}$ is a magnetization-related hysteretic component that saturates (remains constant) for large values of magnetizing current i_{md}. The inductance $L_{m,\mathrm{sat}}$ corresponds to the slope of the magnetizing characteristic at saturation.

The Preisach model is parameterized by the following normal distribution, which corresponds to a statistical distribution of elementary magnetic dipoles of mean value m and width w (Fig. 12)

$$\nu(m,w) = \frac{\lambda_{Ms}}{2\pi\sigma_m\sigma_w} \exp\left\{-\frac{1}{2}\left[\frac{(w-\overline{w})^2}{\sigma_w^2} + \frac{m^2}{\sigma_m^2}\right]\right\}. \tag{15}$$

λ_{Ms} is a constant with dimensions of flux linkage, σ_m and σ_w are standard deviations, and $\overline{w}$ is a mean value. The material's magnetic history divides the Preisach domain in two parts: the upper part $\mathcal{D}^{(-)}$ corresponds to dipoles with negative magnetization; the lower part $\mathcal{D}^{(+)}$ corresponds to positive magnetization. The magnetization component of flux is

$$\lambda_{md,M} = \iint_{\mathcal{D}^{(+)}} \nu(m,w)dmdw - \iint_{\mathcal{D}^{(-)}} \nu(m,w)dmdw. \tag{16}$$

The incremental inductance $L_{mi} = d\lambda_{md,M}/di_{md}$ may be computed from (15) and (16).

The model's state variables are λ_{md} and i'_{fds}; the average-value engine provides the average currents $\overline{i^s_{dr}}$, $\overline{i^s_{qr}}$, and the rate of change $d\overline{i^s_{dr}}/dt$, while v'_{fds} is obtained from the voltage regulator. In summary, the state equations are

$$\frac{d}{dt}\lambda_{md} = \frac{L_{m,\mathrm{sat}} + L_{mi}}{L'_{lfds} + L_{m,\mathrm{sat}} + L_{mi}} \times \left(v'_{fds} - r'_{fds}i'_{fds} + L'_{lfds}\frac{d}{dt}\overline{i^s_{dr}}\right) \tag{17}$$

and

$$\frac{d}{dt}i'_{fds} = \frac{v'_{fds} - r'_{fds}i'_{fds} - (L_{m,\mathrm{sat}} + L_{mi})\frac{d}{dt}\overline{i^s_{dr}}}{L'_{lfds} + L_{m,\mathrm{sat}} + L_{mi}}. \tag{18}$$

For further details about this model, the reader is referred to [3].

REFERENCES

[1] R. W. Ferguson, R. Herbst, and R. W. Miller, "Analytical studies of the brushless excitation system," *AIEE Trans., Part III-B, Power App. Syst.*, vol. 79, pp. 1815–1821, Feb. 1960.

[2] E. C. Whitney, D. B. Hoover, and P. O. Bobo, "An electric utility brushless excitation system," *AIEE Trans., Part III-B, Power App. Syst.*, vol. 79, pp. 1821–1828, Feb. 1960.

[3] D. C. Aliprantis, S. D. Sudhoff, and B. T. Kuhn, "A brushless exciter model incorporating multiple rectifier modes and Preisach's hysteresis theory," *IEEE Trans. Energy Convers.*, to be published.

[4] *Recommended Practice for Excitation System Models for Power System Stability Studies*, IEEE Std. 421.5, Mar. 1992.

[5] R. L. Witzke, J. V. Kresser, and J. K. Dillard, "Influence of A-C reactance on voltage regulation of 6-phase rectifiers," *AIEE Trans., Part I, Commun. Electron.*, vol. 72, pp. 244–253, Jul. 1953.

[6] V. H. Jones and W. J. Bonwick, "Three-phase bridge rectifiers with complex source impedance," *Proc. Inst. Elect. Eng.*, vol. 122, no. 6, pp. 630–636, Jun. 1975.

[7] F. Preisach, "Über die magnetische Nachwirkung," *Zeitschrift für Physik*, vol. 94, pp. 277–302, Mar./May 1935.

[8] E. Della Torre, *Magnetic Hysteresis*, 1st ed. New York: IEEE Press, 1999.

[9] *Test Procedures for Synchronous Machines*, IEEE Std. 115, Dec. 1995.

[10] A. Darabi and C. Tindall, "Brushless exciter modeling for small salient pole alternators using finite elements," *IEEE Trans. Energy Convers.*, vol. 17, no. 3, pp. 306–312, Sep. 2002.

[11] L. Ljung, *System Identification: Theory for the User*. Englewood Cliffs, New Jersey: Prentice-Hall, 1987.

[12] C.-S. Liu, Y.-Y. Hsu, L.-H. Jeng, C.-J. Lin, C.-T. Huang, A.-H. Liu, and T.-H. Li, "Identification of exciter constants using a coherence function based weighted least squares approach," *IEEE Trans. Energy Convers.*, vol. 8, no. 3, pp. 460–467, Sep. 1993.

[13] E. Ludwig, M. L. Crow, K. Erickson, and K. Shah, "A feasibility study of on-line excitation system parameter estimation," *IEEE Trans. Power Syst.*, vol. 13, no. 3, pp. 910–916, Aug. 1998.
[14] C. C. Lee and O. T. Tan, "A weighted-least-squares parameter estimator for synchronous machines," *IEEE Trans. Power App. Syst.*, vol. PAS-96, no. 1, pp. 97–101, Jan./Feb. 1977.
[15] J. J. Sanchez-Gasca, C. J. Bridenbaugh, C. E. J. Bowler, and J. S. Edmonds, "Trajectory sensitivity based identification of synchronous generator and excitation system parameters," *IEEE Trans. Power Syst.*, vol. 3, no. 4, pp. 1814–1822, Nov. 1988.
[16] J.-C. Wang, H.-D. Chiang, C.-T. Huang, Y.-T. Chen, C.-L. Chang, and C.-Y. Huang, "Identification of excitation system models based on on-line digital measurements," *IEEE Trans. Power Syst.*, vol. 10, no. 3, pp. 1286–1293, Aug. 1995.
[17] J. H. Holland, *Adaptation in Natural and Artificial Systems*. Cambridge, MA: MIT Press, 1998.
[18] D. E. Goldberg, *Genetic Algorithms in Search, Optimization, and Machine Learning*. Reading, MA: Addison-Wesley, 1989.
[19] ——, *The Design of Innovation. Lessons From and for Competent Genetic Algorithms*. Norwell, MA: Kluwer, 2002.
[20] F. Alonge, F. D'Ippolito, G. Ferrante, and F. M. Raimondi, "Parameter identification of induction motor model using genetic algorithms," *Proc. Inst. Elect. Eng., Contr. Theory Appl.*, vol. 145, no. 6, pp. 587–593, Nov. 1998.
[21] K. S. Huang, W. Kent, Q. H. Wu, and D. R. Turner, "Parameter identification of an induction machine using genetic algorithms," in *Proc. IEEE Int. Symp. Computer Aided Control System Design*, vol. 1, 1999, pp. 510–515.
[22] H. Razik, C. Defranoux, and A. Rezzoug, "Identification of induction motor using a genetic algorithm and a quasi-Newton algorithm," in *Proc. IEEE Power Electronics Congress CIEP*, Oct. 2000, pp. 65–70.
[23] R. Escarela-Perez, T. Niewierowicz, and E. Campero-Littlewood, "Synchronous machine parameters from frequency-response finite-element simulations and genetic algorithms," *IEEE Trans. Energy Convers.*, vol. 16, no. 2, pp. 198–203, Jun. 2001.
[24] D. C. Aliprantis, S. D. Sudhoff, and B. T. Kuhn, "Experimental characterization procedure for a synchronous machine model with saturation and arbitrary rotor network representation," *IEEE Trans. Energy Convers.*, vol. 20, no. 3, pp. 595–603, Sep. 2005.
[25] P. C. Krause, O. Wasynczuk, and S. D. Sudhoff, *Analysis of Electric Machinery*. New York: IEEE Press, 1995.
[26] D. C. Aliprantis, S. D. Sudhoff, and B. T. Kuhn, "A synchronous machine model with saturation and arbitrary rotor network representation," *IEEE Trans. Energy Convers*, vol. 20, no. 3, pp. 584–594, Sep. 2005.
[27] D. C. Aliprantis, "Advances in electric machine modeling and evolutionary parameter identification," Ph.D. dissertation, Dept. ECE, Purdue Univ., West Lafayette, IN, Dec. 2003.
[28] *Advanced Continuous Simulation Language (ACSL) Reference Manual*, AEgis Technologies Group, Inc., Huntsville, AL, 1999.
[29] K. Deb, *Multi-Objective Optimization Using Evolutionary Algorithms*. Chichester: Wiley, 2001.

Dionysios C. Aliprantis (M'04) received the electrical and computer engineering diploma from the National Technical University of Athens, Athens, Greece, in 1999. He received the Ph.D. degree in electrical and computer engineering from Purdue University, West Lafayette, IN, in 2003.

Currently, he is serving in the armed forces of Greece. His interests include the modeling and simulation of electric machines and power systems, and evolutionary optimization methods.

Scott D. Sudhoff (SM'01) received the B.S. (Hons.), M.S., and Ph.D. degrees in electrical engineering from Purdue University, West Lafayette, IN, in 1988, 1989, and 1991, respectively.

Currently, he is a Full Professor at Purdue University. From 1991 to 1993, he was Part-Time Visiting Faculty with Purdue University and as a Part-Time Consultant with P. C. Krause and Associates, West Lafayette. From 1993 to 1997, he was a Faculty Member at the University of Missouri-Rolla. He has authored many papers. His interests include electric machines, power electronics, and finite-inertia power systems.

Brian T. Kuhn (M'93) received the B.S. and M.S. degrees in electrical engineering from the University of Missouri-Rolla in 1996 and 1997, respectively.

He was a Research Engineer at Purdue University, West Lafayette, IN, from 1998 to 2003. Currently, he is a Senior Engineer with SmartSpark Energy Systems, Inc., Champaign, IL. His research interests include power electronics and electrical machinery.